LOCAL DELAMINATIONS INDUCED BY INTERACTION BETWEEN INTRALAMINAR CRACKING AND SPECIMEN EDGE IN QUASI-ISOTROPIC CF/EP NCF COMPOSITES IN FATIGUE LOADINGS

H. B. Kahla,[1,2] Z. Ayadi,[2] and J. Varna[1*]

Keywords: *delamination, intralaminar cracks, fatigue; stiffness, NCF composite*

Experimental results are presented on the onset and propagation of local delaminations caused by the interaction between specimen edges and intralaminar cracks in fiber bundles of 90° layers in quasi-isotropic [−45/90/45/0]ₛ CF/EP noncrimp fabric (NCF) laminates subjected to tension-tension fatigue loadings. It is confirmed that the first damage mode is intralaminar cracking in 90° layers, which consists of intrabundle cracks and cracks in the matrix between bundles (often beginning from stitches). This damage mode triggers cracking in off-axis layers and local delaminations in positions where the 90° layer crack meets an adjacent layer. The process of local delamination is significantly enhanced at specimen edges, where the out-of-plane edge stresses contribute to the local delamination. During cyclic loadings, delaminations grow and coalesce along the edge and propagate towards the specimen center. These processes are quantified experimentally at different levels of cyclic load. In a low-stress fatigue, a very high number of cycles is required to detect small edge delaminations, and they stay at the edge. In high-stress cyclic tests, delaminations grow faster inside the composite: about 20% of the interface in the central zone can be delaminated. It is found that the reduction in the axial modulus is proportional to the relative delaminated area, proving that delamination is the major stiffness reduction factor in these laminates.

[1]Department of Engineering Sciences and Mathematics, Luleå University of Technology, SE-97187, Luleå, Sweden
[2]Institut Jean Lamour, SI2M, Université de Lorraine, EEIGM 6 Rue Bastien Lepage, F-54010 Nancy, France
[*]Corresponding author; tel.: +46 739405754; e-mail: janis.varna@ltu.se

Introduction

The large variation of parameters in composites (fibers, matrices, volume fractions of constituent, reinforcement architectures on different scales, layer stacking sequences, manufacturing methods,…), the time-consuming and limited characterization tools and methods, together with the current lack of reliable multiscale models, prevent one from using one general approach to predicting the behavior of all composites. Noncrimp fabric (NCF) composites, considered as a compromise between straight-fiber prepreg tape and "crimped" woven composites, are known for their good mechanical properties and the relatively easy and cost-effective production. The investigations carried out on NCF laminates demonstrate their complex and sometimes unexplained behavior [1-3], which emphasizes the necessity for a better understanding of mechanisms of their damage and their growth under different loading conditions, and for the development of reliable methods to describe the effect of damage on the integrity of structure of these composites.

The damage development in NCF composites under different quasi-static loads and the influence of damage on their residual properties have been investigated in many papers. For example, Mattsson et al. [2] studied the damage behavior of cross-ply NCF composites under tensile loadings and investigated the dependence of their mechanical properties on the stacking sequence. Edgren et al. [4] quantified different cracking modes in NCF laminates and performed a stress state analysis by the FEM, showing that, due to the bundle mesostructure, the out-of-plane stress at layer interfaces are high.

Mikhaluk et al. [5] investigated the damage initiation and evolution in quasi-isotropic NCF composites under tensile loads and developed a finite-element model to predict the growth of damage. They observed a correlation between damage zones and the resin-rich zones created by the stitching pattern. Therefore, parameters related to the stitching pattern have to be considered for a comprehensive analysis of damage in NCF composites, which makes the analysis even more complicated. Extensive studies of biaxial and quadriaxial NCF composites in different types of quasi-static loading are published by Lomov et al. [3, 6-8].

The behavior of NCF composites in fatigue loadings is studied much less. Vallons et al. [3] investigated the behavior of biaxial NCF composites in tension-tension fatigue and their postfatigue behavior. Testing specimens of $[0/90]_s$, $[90/0]_s$, and $[45/–45]_s$ orientations with respect to the axial loading direction, they used the X-ray radiography for detailed studies of intralaminar crackings in 90° bundles. Peculiar was the observation that the surface 90° bundles did not have intrabundle cracks. Another unusual phenomenon was found in CF/EP NCF $[+45/–45/0/90]_s$ composites: early delamination in the middle of the 90° layer [9]. It grew rapidly, dividing the sample into two halves, kept together by the clamped end tabs. The intralaminar cracking in high-temperature CF/polyimide 8-harness quasi-isotropic laminates in thermal cycling was studied in [10], and the intrabundle crack density in different layers versus the number of thermal cycles was determined. In [11], the tensile fatigue behavior of a biaxial NCF composite was investigated for stresses similar to the damage initiation stress in 90° bundles detected by acoustic emission in a quasi-static test. It was found that numerous intralaminar cracks developed during the cycling, showing a strong fatigue effect, while the decrease in the tensile modulus was very small.

Whether it is a quasi-static or cyclic tensile loading, the damage mechanisms are similar, and the most common damage modes in continuous-fiber composites are intralaminar cracking, delamination, and fiber breakage [12]. These modes can arise separately or can interfere, either bolstering or delaying or even arresting each other.

Interlayer delaminations usually start at specimen edges, and the presence of intralaminar cracks meeting the interface significantly accelerates this process. Many papers have been written discussing the delamination resistance of CFRP laminates [13-16]. The effect of the delaminations locally originating from intralaminar cracks on the stiffness reduction in prepreg tape $[0_m/90_n]_s$ laminates was analyzed, for example, in [17]. Takeda and coworkers [18, 19] performed a shear-lag analysis to calculate the Energy Release Rate (ERR) for the growth of delamination in CFRP prepreg tape cross-ply laminates. In the above studies, the effect of specimen edge, where a delamination usually starts, was not included. For quasi-static loadings of prepreg tape laminates, the onset and growth of edge delamination, considering the effects of intralaminar cracks, was investigated in [20, 21]. In [10], the rise and growth of an edge delamination under cyclic loadings by over 100 M cycles, considering the edge-crack interaction, was studied on quasi-isotropic $[45/0/–45/90]_s$ CFRP specimens. Analyzing the ERR, it was found that a certain critical crack density had to be reached before the growth of de-

lamination took over and the cracking decayed. It was also found that the growth rate of edge delamination with number of cycles followed the Paris law.

In [13], the delamination growth from transverse cracks in carbon-fiber-reinforced polymer-matrix composites was studied, and it was found that delaminations of approximately the same size developed from both tips of an intralaminar crack in cases where the delamination was of almost pure Mode II. In the case of a nonsymmetric mesogeometry (including staggered cracks), the fracture mode changed, and delaminations on different sides of the same intralaminar crack grew differently. They also showed that the growth of delamination rate followed the Paris law. The same law for the propagation of an interface crack was experimentally confirmed and modelled in [22,23] on a much lower fiber debond scale.

In [12], applying the optical microscopy, SEM, and X-ray computed tomography (CT) to more complex architectures than NCF laminates (3D woven), authors found that the delamination between stitch yarns and the surrounding material was very significant. In surface layers, the first intralaminar cracks were found in the matrix between bundles. Many cracks in the matrix channels between bundles were also found in other studies [24-27] on 3D woven composites — they were in the resin-rich channel between tows inside the material. It seems that, even in 3D woven composites, the most probable origin of delamination is an intralaminar crack; however, large delaminations may also start from local delaminations between yarns and from longitudinal cracks in the stitch yarn. Similar features were observed in the fatigue loading of plain weave composites [27], where cracks in the transverse fiber bundles appeared first, then being deflected to cause delaminations.

The brief review presented shows the differences and similarities in damage patterns arising during tension-tension cyclic loading in NCF reinforced composites and in the much more complex woven fabric composites. The most typical sequences of damage development leading to large delaminations seem to be related to specimen edge interactions with intralaminar (intra- or interbundle) cracks in layers. Nevertheless, due to the great variations and different combinations of geometrical and mechanical properties, we are currently still far from the complete understanding of different effects and are even more distant from reliable simulations and predictions regarding delaminations in damaged NCF laminates.

We hope that the current paper, which presents data and analysis results for the damage development in carbon fiber/epoxy $[-45/90/45/0]_s$ NCF laminates in cyclic tension-tension loadings, will contribute to a better understanding of matrix-related fatigue phenomena. The intralaminar cracking development in layers of the laminate and its effect on local delaminations (starting from cracks) in interaction with the specimen edge are analyzed, and the effect of different damage modes on the laminate stiffness are estimated.

1. Experimental Procedures

2.1 Description of materials

Quasi-isotropic $[-45/90/45/0]_s$ NCF carbon fiber/ HTS40/RTM6 epoxy laminates, manufactured at 180°C and consisting of unidirectional (UD) weave layers with 12K fiber bundles (see Fig. 1), were studied. The areal density of a layer was 242 g/m^2, but the bundle width and thickness in the composite were 3.5 and 0.25 mm, respectively. Bundles in the UD weave were kept together by two sets of stitches (see Fig. 1). Table 1 shows the elastic properties of the corresponding UD composite. The average longitudinal modulus of the $[-45/90/45/0]_s$ specimens was 43.7 GPa, which correlated well with the value of 46 GPa obtained analytically using the Classical Laminate Theory (CLT) and the elastic properties of UD composite E_L = 120 GPa, E_T = 9.18 GPa, G_{LT} = 9.94 GPa, γ_{LT} = 0.311, α_L = 0.32·10^{-6} °C^{-1}, and α_T = 3.16·10^{-6} °C^{-1}.

Specimens of length 180 mm were cut from the plates produced. Both their edges were polished using a sequence of sand papers (P240, P600, P1200, P2500, and P4000) and then by a liquid diamond slurry (with 9- to 0.25-μm particles). The specimens were about three bundle width wide: their width w was approximately 10 to 12 mm after grinding and polishing. The 10-kN loading capacity was the main limiting factor for selecting this width. Wider specimens would have a lower scatter in the stiffness and in the degree of damage development.
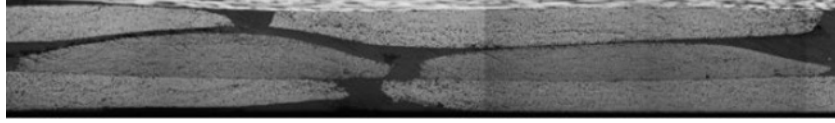
Fig. 1. Optical micrograph of the bundle structure observed at the edge of a quasi-isotropic $[-45/90/45/0]_s$ laminate.

Since GFRP end tabs were glued to each specimen by an Araldite 2011 two-component epoxy adhesive, the gage length was 100 mm.

2.2 Experiments

2.2.1. Cyclic loading parameters. In cyclic loadings, a test frequency of 5 Hz was used, which is typically selected to avoid the internal heating of the composite [28]. The tests were performed keeping the maximum stress constant in cycles with a sinusoidal waveform and with the ratio of the minimum to maximum stresses in the cycle $R = 0.1$. Using an ElectroPulsTM E10000 Linear-Torsion machine with a 10-KN load capacity, the cyclic testing was carried out at several maximum stress levels, which were determined before cycling in a quasi-static tensile pretest with a displacement rate of 2 mm /min, individually for each used specimen, to correspond to the strain levels of 0.4, 0.45, 0.5, 0.55, and 0.6%. The axial modulus was determined from the slope of the stress–strain curve within the strain interval of 0.05-0.25%. After each block of cycles, it was remeasured in the same strain interval. The longitudinal strain in the pretest was measured using an extensometer with a 50-mm gage length.

The test was stopped after each block of cycles ($\Delta N = 1, 10, 10^2, 10^3, 10^4, \ldots$), and edge replicas were taken. The final block was shorter or equal to 1-M cycles, which is the typical limit for laboratory cyclic testings. After each block of cycles, the damage state (the crack density in layers and the delamination length along different interfaces) at both edges of the specimen was determined by a microscopic analysis of the edge replicas reproducing the surface topography of specimen. Since the use of replicas, the specimen was not removed from the machine, and its alignment with the loading direction did not change. This technique is suitable for measuring small changes in the axial modulus of laminates in the quasi-elastic manner described above. At least three specimens were used for each level of strain in the cyclic loading.

2.2.2. Microdamage characterization. The respective number of cracks n_i over the distance $L = 50$ mm in the layer with an index i was counted, and the crack density ρ_i was calculated as

$$\rho = n_i / (L \cdot \sin \theta_i), \tag{1}$$

where θ_i is the fiber orientation angle in the ith layer considered.

The delamination length l_d was defined as the total length of all local delaminations on one interface on the specimen edge, measured over the distance L, in the same region where the strain for stiffness reduction and the crack density were measured. The largest delaminations were observed at interfaces between the 90 and ±45° layers. Since, delaminations at the 45°/0° interface were very small and arose only at very high loadings, they were not quantified. After each loading step, the delaminations at the –45°/90° and 90°/45° interfaces, denoted further as $l_{-45/90}$ and $l_{90/45}$, were determined in measurements at both edges of each specimen. Due to symmetry, we have two interfaces of a certain type (–45°/90° or 90°/45°) for each edge in the $[-45/90/45/0]_s$; actually, for each type of interface, the delaminations were measured over the distance of $4 \times 50 = 200$ mm, which, as will be shown in Sect. 3, is rather representative.
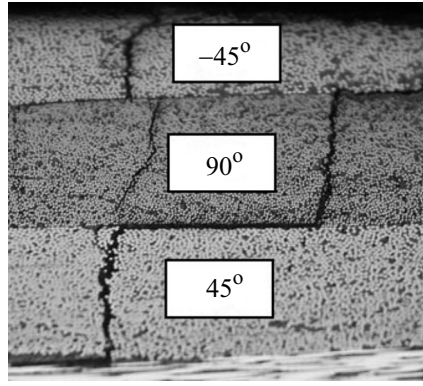
Fig. 2. Example of the damage state in the lower part of a $[-45/90/45/0]_s$ laminate after 1 M cycles in a 0.55% strain loading.

The relative delamination length is presented as the ratio between delamination and interface lengths, namely,

$$l_{drel} = \frac{l_d}{4L}, \qquad (2)$$

where $d = -45°/90°$ or $90°/45°$.

Usually, the delamination length l_d at the specimen edge is not representative compared with that inside the specimen. To evaluate it in the bulk of the material, one edge of the specimen was grinded stepwise and then polished and examined under a Nikon Eclipse MA200 microscope equipped with a DS-U3 camera control unit and a NIS-Elements software. Since this method is destructive, it was applied to specimens only after the final cyclic loading block. This type of destructive sectioning was also used in [29] to quantify the damage as a function of fatigue cycles.

3. Results and Discussion

The following discussion will be referred to x and y axes, where x is in the loading direction and y is in the specimen width direction. Although the damage modes were the same for both NCF and prepreg tape laminates, the damage prediction in NCF composites, due to their heterogeneous mesostructure, was much more complex. In contrast to prepreg tape composites, the damage state in NCF composites is affected by the stitching pattern and the layer mesostructure containing bundles. Both of them lead to local stress concentrations, and, therefore, the first damage appeared as intralaminar cracks in the 90° layer in positions coinciding with stitch positions. In [12], for a 3D woven composite, it was also found that the debonding between the stitch yarns and the surrounding material was the main damage onset mechanism.

With increasing number of cycles, cracks arouse at more random, not stitch-related, positions inside a bundle (actually, these positions were governed by the Weibull strength distribution). At higher crack densities and at a greater length of local delamination, the intralaminar cracking slowed down due to the weakened stress field between existing cracks. The 90° layer intralaminar cracks generated interlaminar stresses at crack tips, promoting the initiation of a local delamination at the interface with ±45° layers. The stress magnification in layers adjacent to the cracked 90° layer in local regions were the 90° cracks are located is the reason for the formation of an early short intralaminar crack in adjacent off-axis layers (see Fig. 2). Due to their geometrical appearance, in damaged tape laminates, they are often referred to as "stitch cracks" (not to be mixed with stitches in the current paper) [30]. In our material, these cracks were not "tunnels" that would cover the whole width of specimen. With increasing number of cycles, they slowly grew outside the local stress concentration region [31]. The 45° layer cracks may also start from stress concentrations or material imperfections created by transverse stitches (at the interface) or
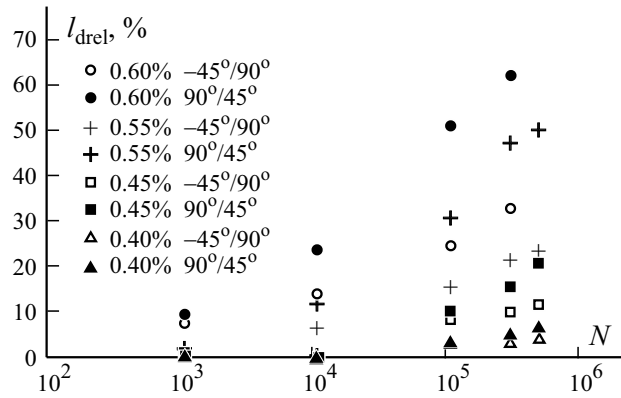
Fig. 3. Evolution of the relative delamination length l_{drel} with number of cycles N. Load levels and the particular interface are indicated in the legend. (All specimens were subjected to not more than 1 M cycles, except for the case of 0.6% strain, where the specimen was subjected to 0.3 M cycles).

longitudinal stitches (in-between bundles) in the layer. In our material, cracks in the 90° layer, after their origination, usually propagated very rapidly from one specimen edge to another, building well-defined tunnels.

The 90° crack induced delamination and cracking in adjacent off-axis layers take place almost simultaneously. Since the crack plane in the 45° layer is oriented at 45° to the 90° crack plane, the 45° layer crack was seen shifted with respect to the 90° crack. The shifting distance depends on how far the onset point of this particular 45° layer crack has been from the edge. A couple of cracks (one in the 90° layer and another one in the 45° layer) crossing close to the edge accelerates the delamination between these cracks which, in the x, y plane has the form of a triangle connected with the free edge.

Hosoi and al. [32] detected a similar damage sequence in a [45/0/–45/90]$_s$ CFRP by optical edge observations and using a soft X-ray photography: edge delaminations started only in local regions with intralaminar cracks in the 90° layer. It is interesting that, in [10] delamination did not start from a single precrack introduced in a quasi-static manner before the fatigue test, which according to authors, pointed to some difference in the geometry of the quasi-static crack or to the necessity for a certain crack density. However, one difference from our observations has to be mentioned: we did not observe coalescence of all local delaminations and such extremely large delaminated areas as in [10].

3.1. Local delaminations at the specimen edge

A local edge delamination in the presence of intralaminar cracks is caused by high out-of-plane stresses (some of them may be singular in a linear elastic analysis) at the interface in the edge region: a) σ_{zz} and σ_{xz} and high corresponding Mode I and Mode II ERRs for growth along the edge and b) σ_{xz} and σ_{zz} for propagation inside the specimen. For the different specimens tested, delaminations without any connection with intralaminar cracks were observed rarely. Figure 3 shows the growth in the relative delamination length, measured on the edge at the –45°/90° and at the 90°/45° interfaces, with the number of fatigue cycles N. The l_{drel} was measured separately on the two edges (A and B) of one specimen for each loading case. The similarity of the values found for both edges confirms the representativeness of the measurement. Therefore, in the following, the values of l_{drel} presented correspond to the average of delamination length on both edges.

In low-stress fatigue tests (at strains 0.45%), the delamination started after more than 50,000 cycles, growing slowly with increasing number of cycles. For example, less than 10% of the specimen edge was delaminated after 1M cycles in the 0.4% strain test. The final values of l_{drel} were in the same range as in a quasi-static loading test at a 1% strain performed on specimens of the same lay-up (unpublished results).
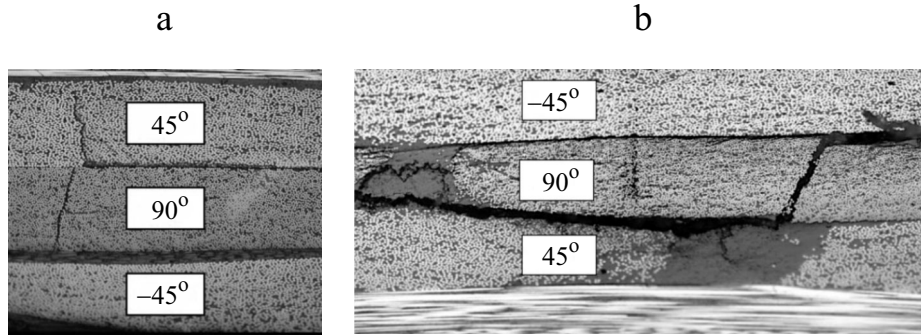
Fig. 4. Features of local delaminations in: a) low-strain cyclic loading and b) high-strain cyclic loading.

At higher cyclic stresses, large delaminations developed. Measurable delaminations started already after 1000 cycles. The growth of delamination rate increased with the cyclic stress applied. For example, the delamination length reached after 1M cycles at a 0.4% strain required only 1000 cycles at a 0.6% strain.

There was a clear difference between the development of delaminations at the –45°/90° and at 90°/45° interfaces (see Fig. 3): the delamination length was significantly greater at the 90°/+45° interface. This difference cannot be explained by different crack densities in the +45° and –45° layers. At a high crack density in the 90° layer, we observed more cracks in the –45° layer than in the +45° one. Nevertheless, the delaminations at the 90°/45° interface were larger. It seems unlikely that cracks in the 45° layer being close to 90° cracks would delay delamination. Nevertheless, this indicates that the interaction between 90° cracks and 45° cracks does not accelerate local delaminations and is not the reason for larger delaminations. A 3D FEM analysis of edge stresses in an undamaged laminate with homogeneous layers did not show any significant difference in stresses at both interfaces. The stitch patterns on both types of interfaces were also identical. Hence, the reason for the larger delaminations at the 90°/45° interface remained unclear. Apparently, a 3D FEM analysis, with cracks in several layers, having a bundle mesostructure, meeting the edge is required to explain these observations. Based on fracture mechanics, O'Brien [33], argued that the growth of edge delamination can occur at different ratios of fracture modes (I, II, and III), depending on the laminate lay-up and loading conditions. Therefore, the stitched structure, combined with the intralaminar cracking state at the edge, and the interaction between different damage modes could be the reason for the difference observed.

Some additional features can be seen in Fig. 4. In a low-strain fatigue loading, a local delamination starting from the intralaminar crack tip at one interface (for example, between the 90°/45° layers) prevents the origination and propagation of a symmetric (with respect to the crack) delamination of the same interface. Prevented is also the delamination on the same side of the crack, but on the other interface (–45°/90° in the example considered). Usually, delaminations migrate from one interface to another through an intralaminar crack in the 90° layer (Fig. 2). At higher strain levels in fatigue (0.55% and above) or at a high number of cycles, the pattern changed, and delaminations were observed on both interfaces, (Fig. 4b), but they did not grow in the same way as in Fig. 2. This could be caused by a greater number of cracks and longer local delaminations. The interaction between multiple delaminations alters the rate of strain energy release at the tip of the original delamination crack [34]. The imperfect mesostructure of the layer (bundles do not have a rectangular crosssection and are not perfectly aligned) enhances the irregularity comparing with that in very symmetric delaminations, as shown in [13]. Alderliesten et al.[35] reported the loss of symmetry when intralaminar cracks in different layers staggered and the delamination proceeded in a mixed mode instead of Mode II. They noticed that, in this case, the propagation of delamination on the opposite side of the separating layer was prevented until the first delamination reached a length of about 2 to 3 mm.

Figure 5 shows the evolution of a total edge delamination with growing number of cycles (in logarithmic axes). Apparently, it does not follow the Paris law, which predicts a linear dependence on the number of cycles in a steady state region at certain value of ERR. In order to understand the significance of crack density in this process, we calculated the delamination length corresponding to one hypothetical intralaminar crack by using l_{drel} and crack density ρ_{90} in this calculation. Comparing different stress levels, there was found no systematic relation reminding the Paris law. It seems that the simple procedure
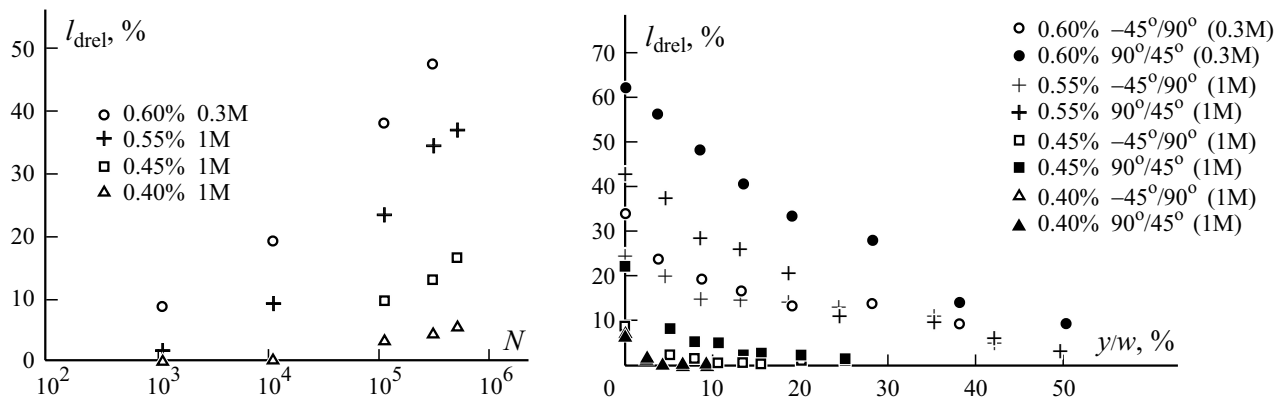
Fig. 5. Growth in the relative delamination length l_{drel} on the edge with number of cycles N (average over both interfaces).

Fig. 6. Relative delamination length l_{drel} at the –45°/90° and 90°/45° interfaces as a function of the relative distance y/w from the edge.

introducing a delamination per one hypothetical crack is not good, because different cracks appear after different number of cycles and the time for growth of an individual debond is very different. Other factors making the situation very complex is the mesostructure, which makes a pure Mode II propagation in the steady state questionable, and the close presence of other cracks with their own local delaminations.

3.2. Delamination depth (dependence on distance from the edge)

Interior delaminations (far from specimen edges) could be initiated by manufacturing defects, e.g., incomplete curing or voids between layers, but, most probably, from local stress concentrations in the vicinity of the intralaminar cracks created during a cyclic loading. Since the out-of-plane stress state in the edge region is severe and the above-mentioned imperfections and damage are equally typical of the edge region and the interior, the growth of interlayer delaminations along the interface from the edge region inside the specimen can be expected. In other words, the relative delamination length can depend on its "depth," which is the distance from the edge in the y direction, the relative delamination length being greatest at the specimen edge.

To inspect this guess, one specimen edge was grinded gradually, then polished as described in Sect. 2, and analyzed using an optical microscope.

As shown in Fig. 6, at low levels of fatigue stress (under a 0.45% strain), local delaminations developed close to the edge and vanished rapidly within the first millimeter from it. The delamination did not grow deeper inside even at high numbers of cycles. Similar behavior was observed in the quasi-static loading at a high strain (unpublished results). For higher fatigue stresses, delaminations arose not only at the edge, but l_{drel} was consistently greater at the edge. The higher the fatigue stress, the deeper delaminations grew into the material. The dependence on the depth coordinate was roughly linear. In a specimen subjected to 0.3 M cycles at a 0.6% strain about 60% of its 90°/45° interface at the edge was delaminated, whereas only 20% of it was delaminated in the middle of the specimen. A specimen subjected to 1 M cycles at a 0.55% strain, at the same interface, had a lower relative delamination length at the edge (43%), and the relative delamination length dropped to about 4% in its middle. The above-discussed feature that the relative delamination length on the edge was systematically greater at the 90°/+45° interface than at the –45°/90° one, also showed up inside the specimen.
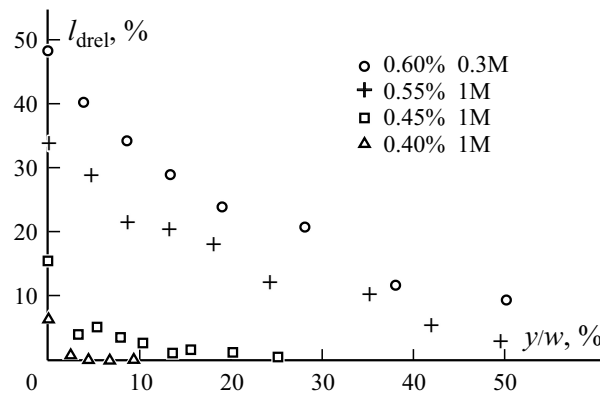
Fig. 7. Delamination length l_{drel} averaged over both interfaces as a function of the relative distance y/w from the edge.

Despite the difference in delamination lengths between −45°/90° and 90°/45° interfaces, the effect of both types of delamination on the laminate stiffness was expected to have a similar character: they will reduce the participation of involved layers in sharing the load. Therefore, in Subsect. 3.3, in order to simplify the analysis, the stiffness reduction will be correlated with the average of delamination lengths at these two interfaces. The average delamination length on the edge versus the number of cycles at different levels of loading is shown in Fig. 5, but its distribution along the specimen width is shown in Fig. 7.

3.3. Reduction in the axial modulus E_x

The degradation in the axial modulus E_x was measured before and after each block of cycling, as described in Sect. 2, and results for some selected specimens are shown in Fig. 7. The simultaneous development of several damage modes and their interaction make it difficult to assess the contribution of each mode to the stiffness reduction. For example, local delaminations increased the opening and sliding displacements of intralaminar cracks, and, therefore, these cracks reduced the stiffness much more than cracks without delaminations; when the delaminations at both interfaces were large, the cracked layer separated from the rest of the laminate, and crack density in the layer lost its importance.

The importance of intralaminar cracks on the stiffness reduction can be estimated using the CLT together with the modified ply-discount model, which assumes zero values for the transverse and shear modulus in damaged layers (this corresponds to the infinite density of intralaminar cracks). Assuming the infinite crack density in the 90° layer and using the CLT, the axial modulus of the quasi-isotropic laminate dropped only by 4%, which was much less than the experimentally observed reduction at high loads, but was comparable with modulus reduction in the low-stress fatigue, which is also shown in Fig. 8. It has to be noted that the so-called normalized crack density, defined as the ratio between the layer thickness and the distance between cracks, was very far from infinite: it reached 0.1 after 1 M cycles at a 0.5% strain. In addition, the assumption that the 45° layers of both orientations also have an infinite number of intralaminar cracks and using the CLT, led to a 13% reduction in the axial modulus of laminate. Although this value was closer to the measured stiffness reduction in the high-cycle tests performed, the actual crack density was not high, and the predicted reduction in the axial modulus was still much smaller than that found in the high-stress cyclic loading (see Fig. 8, where this reduction reaches 20%). Obviously, large delaminations in a high-stress loading influence the stiffness degradation very strongly. Therefore, in Fig. 9, the axial modulus is shown as a function of the relative delamination length on the edge. To qualitatively explain this rather linear relationship, we approximated the delamination length as a function of the relative distance y/w from the specimen edge shown in Fig. 7 by a linear function (assuming a triangle form for the delaminated area), and found that the delaminated area was roughly proportional to the delamination length on the edge. Thus, the results shown in Fig. 9
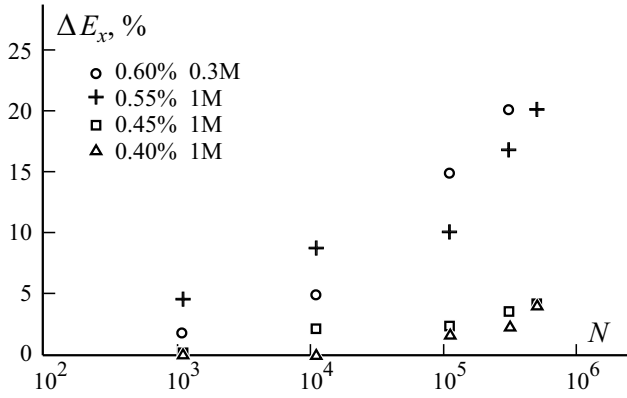
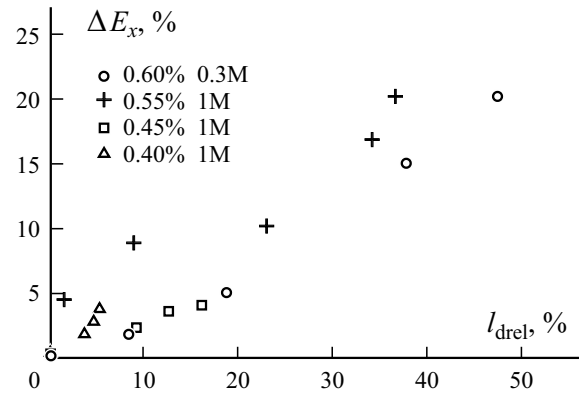Fig. 8. Reduction ΔE_x in the axial modulus with number of cycles N.

Fig. 9. Reduction ΔE_x in the axial modulus versus the relative delamination lengths l_{drel} on the edge averaged over both interfaces.

can be interpreted as the reduction in the axial modulus, which is almost proportional to the delaminated area. This points to the rule-of-mixture (RoM) type of behavior: in the part of laminate where the delamination has led to the almost full separation between layers, some layers had not participated in sharing the load even in the fiber direction.

Therefore, we assume that, in the region of width w_d close to the edge, the –45°/90°/+45° sublaminate is separated from the 0°layer and is not participating in sharing the load (even the longitudinal stress in these layers is zero, and therefore $E_L = E_T = G_{LT} = 0$). In the middle region of laminate, all layers is assumed to act in the longitudinal direction, and the ply-discount model is employed only for the transverse and shear moduli of the damaged layers ($E_T = G_{LT} = 0$). The use of CLT for each region separately gave that $E_x = 0.65 E_{x0}$ and $E_x = 0.87 E_{x0}$ The reduction in the axial modulus for the whole laminate was found by the RoM. According to Fig. 7, approximately 25% of the interface was delaminated at the end of the 0.60% strain cyclic loading, and the RoM gave an axial modulus of the laminate equal to 0.81 of its initial value. The 19% estimated reduction is rather close to the measured maximum reduction in the modulus for the loading case shown in Fig. 9.

Very similar reduction rates in the axial modulus with delamination length can be observed in Fig. 9 for different test conditions (the maximum stress and the number of cycles).

2. Concluding Remarks

This paper presents experimental results of an investigation into the delamination growth starting from intralaminar cracks in CF/EP quasi-isotropic $[-45/90/+45/0]_s$ NCF laminates. A damage development analysis of tension-tension cyclic tests has led to the following conclusions.

- The first mode of microdamage was always the intralaminar (intra- and interbundle) cracking in 90° layers. Almost immediately, it triggered two other mechanisms: a) formation of small crack in adjacent off-axis layers in local stress concentration regions in the vicinity of a crack in the 90° layer and b) local delaminations in the same region.

- The delaminated area and the length of 45° layer cracks grew during cyclic loading. So also did the crack density in the 90° layer. For a currently unknown reason, the delaminated area between the 90°/+45° layers was consistently larger than at the –45°/90° interface.

- Local delaminations were more pronounced in the specimen edge region, at high stresses, and at great numbers of cycles, reaching almost 60%.

- Two patterns of fatigue behavior, dependent on the level of fatigue stress, could be distinguished: in a high-stress fatigue, the zone with delaminations propagated across the whole width of specimen; in a low-stress fatigue, delaminations arose only at the edge.

- The reduction in the axial modulus was proportional to the delaminated area, showing that the delamination was the major factor. This effect can be estimated using the ply-discount model in different its modifications: in some layers, only the transverse and shear moduli were reduced by cracking, whereas in regions where layers weare fully separated from the laminate, even the longitudinal modulus of the layer was zero.

REFERENCES

1. D. Mattsson, R. Joffe, and J. Varna, "Methodology for characterization of internal structure parameters governing performance in NCF composites," Composites: Part B, **38**, No. 1, 44-57 (2007).
2. D. Mattsson, R. Joffe, and J. Varna, "Damage in NCF composites under tension: effect of layer stacking sequence," Eng. Fracture Mechanics, **75**, No. 9, 2666-2682 (2008).
3. K. Vallons, S. V. Lomov, and I. Verpoest, "Fatigue and post-fatigue behaviour of carbon/epoxy noncrimp fabric composites," Composites: Part A, **40**, No. 3, 251-259 (2009).
4. F. Edgren, D. Mattsson, L. E. Asp, and J. Varna, "Formation of damage and its effects on noncrimp fabric reinforced composites loaded in tension," Compos. Sci. Technol., **64**, No. 5, 675-692 (2004).
5. D. S. Mikhaluk, T. C. Truong, A. I. Borovkov, S. V. Lomov, and I. Verpoest, "Experimental observations and finite element modelling of damage initiation and evolution in carbon/epoxy noncrimp fabric composites," Eng. Fracture Mechanics, **75**, No. 9, 2751-2766 (2008).
6. S. V. Lomov, E. B. Belov, T. Bischoff, S. B. Ghosh, T. T. Chi, and I. Verpoest, "Carbon composites based on multiaxial multiply stitched preforms. Part 1. Geometry of the preform," Composites: Part A, **33**, No. 9, 1171-1183 (2002).
7. S. V. Lomov, I. Verpoest, M. Barburski, and J. Laperre, "Carbon composites based on multiaxial multiply stitched preforms. Part 2. KES-F characterisation of the deformability of the preforms at low loads," Composites: Part A, **34**, No. 4, 359-370 (2003).
8. S. V. Lomov, M. Barburski, T. Stoilova, I. Verpoest, R. Akkerman, R. Loendersloot, and R. H. W. Ten Thije, "Carbon composites based on multiaxial multiply stitched preforms. Part 3: Biaxial tension, picture frame and compression tests of the preforms," Composites: Part A, **36**, No. 9, 1188-1206 (2005).
9. N. J. Pagano and G. A. Schoeppner, "Delamination of Polymer Matrix Composites: Problems and Assessment," in A. Kelly and C. Zweben (Eds.), Comprehensive Composite Materials, 433–528, Elsevier (2000).
10. J. Varna and H. Zrida, "Analysis of microdamage in thermally aged CF/polyimide laminates," Mech. Compos. Mater., **53**, No. 1, 45-58 (2017).
11. K. Vallons, M. Zong, S. V. Lomov and I. Verpoest, "Carbon composites based on multi-axial multi-ply stitched preforms–Part 6. Fatigue behaviour at low loads: Stiffness degradation and damage development," Composites: Part A, **38**, No. 7, 1633-1645 (2007).
12. M. Hojo, S. Matsuda, B. Fiedler, T. Kawada, K. Moriya, S. Ochiai, and H. Aoyama, "Mode I and II delamination fatigue crack growth behavior of alumina fiber/epoxy laminates in liquid nitrogen," Int. J. of Fatigue, **24**, No. 2-4, 109-118 (2002).
13. A. J Brunner, S Stelzer, G. Pinter, and G. P. Terrasi, "Cyclic fatigue delamination of carbon fiber-reinforced polymer-matrix composites: Data analysis and design considerations," Int. J. of Fatigue, **83**, 293-299 (2016).

14. A. J. Brunner, "Fracture mechanics characterization of polymer composites for aerospace applications," In P. E. Irving and C. Soutis (Eds.) Polymer composites in the aerospace industry, 191-230, Woodhead Publishing (2015).

15. A. J. Brunner, B. R. K. Blackman, and P. Davies, "A status report on delamination resistance testing of polymer–matrix composites," Eng. Fracture Mech., **75**, No. 9, 2779-2794 (2008).

16. ASTM D 6671-13. Standard Test Method for Mixed Mode I-Mode II Interlaminar Fracture Toughness of Unidirectional Fiber Reinforced Polymer Matrix Composites.

17. M. Kashtalyan and C. Soutis, "The effect of delaminations induced by transverse cracks and splits on stiffness properties of composite laminates," Composites: Part A, **31**, No. 2, 107-119 (2000).

18. N. Takeda and S. Ogihara, "Initiation and growth of delamination from the tips of transverse cracks in CFRP cross-ply laminates," Compos. Sci. Technol., **52**, No. 3, 309-318 (1994).

19. N. Takeda, S. Ogihara, and A. Kobayashi, "Microscopic fatigue damage progress in CFRP cross-ply laminates," Composites, **26**, No. 12, 859-867 (1995).

20. J. Zhang, C. Soutis, and J. Fan, "Effects of matrix cracking and hygrothermal stresses on the strain energy release rate for edge delamination in composite laminates" Composites, **25**, No. 1, 27-35 (1994).

21. L. Y. Xu, "Interaction between matrix cracking and edge delamination in composite laminates," Compos. Sci. Technol., **50**, No. 4, 469-478 (1994).

22. A. Pupurs and J. Varna, "Fracture mechanics analysis of debond growth in a single-fiber composite under cyclic loading," Mech. Compos. Mater., **47**, No. 1, 109-124 (2011).

23. A. Pupurs, S. Goutianos, P. Brondsted, and J. Varna, "Interface debond crack growth in tension–tension cyclic loading of single fiber polymer composites," Composites: Part A, **44**, 86-94 (2013).

24. A. P. Mouritz and B. N. Cox, "A mechanistic interpretation of the comparative in-plane mechanical properties of 3D woven, stitched and pinned composites," Composites: Part A, **41**, No. 6, 709-728 (2010).

25. S. A. Rudov-Clark and A. P. Mouritz, "Tensile fatigue properties of a 3D orthogonal woven composite," Composites: Part A, **39**, No. 6, 1018-1024 (2008).

26. A. P. Mouritz, "Tensile fatigue properties of 3D composites with through-thickness reinforcement," Compos. Sci. Technol., **68**, No. 12, 2503-2510 (2008).

27. S. D, Pandita, G. Huysmans, M. Wevers, and I. Verpoest, "Tensile fatigue damage development in plain weave and knitted fabric composites (GFRP)," Proc. of the 12th Int. Conf. on Composite Materials (ICCM 12), Paris, France, 5-9 (1999).

28. J. Zangenberg and P. Brøndsted "Fatigue life in textile composites used for wind energy engineering", in V. Carvelli and S. V. Lomov (Eds) Fatigue of Textile Composites, Woodhead Publishing (2015)

29. K. H. Tsai, C. H. Chiu, and T. H. Wu, "Fatigue behavior of 3D multi-layer angle interlock woven composite plates," Compos. Sci. Technol., **60**, No. 2, 241-248 (2000).

30. V. T. Bechel, M. Negilski, and J. James, "Limiting the permeability of composites for cryogenic applications," Compos. Sci. Technol., **66**, No. 13, 2284-2295 (2006).

31. H. B. Kahla, Z. Ayadi, F. Edgren, A. Pupurs, and J. Varna, "Statistical model for initiation governed intralaminar cracking in composite laminates during tensile quasi-static and cyclic tests," Int. J. of Fatigue, **116**, 1-12 (2018).

32. A. Hosoi, N. Sato, Y. Kusumoto, K. Fujiwara, and H. Kawada, "High-cycle fatigue characteristics of quasi-isotropic CFRP laminates over 108 cycles (initiation and propagation of delamination considering interaction with transverse cracks)," Int. J. of Fatigue, **32**, No 1, 29-36 (2010).

33. T. K. O'Brien, "Characterization of delamination onset and growth in a composite laminate," In Damage in Composite Materials: Basic Mechanisms, Accumulation, Tolerance, and Characterization. ASTM International (1982).

34. B. Yu, R.S. Bradley, C. Soutis, P. J. Hogg, and P. J. Withers, "2D and 3D imaging of fatigue failure mechanisms of 3D woven composites," Composites: Part A, **77**, 37-49 (2015).

35. R. C. Alderliesten, J. Schijve, and S. Van der Zwaag, "Application of the energy release rate approach for delamination growth in Glare," Eng. Fracture Mech., **73**, No. 6, 697-709 (2006).